An apoptosis-dependent checkpoint for autoimmunity in memory B and plasma cells

Christian T. Mayer[a,1], Jan P. Nieke[b], Anna Gazumyan[b], Melissa Cipolla[b], Qiao Wang[c], Thiago Y. Oliveira[b], Victor Ramos[b], Sébastien Monette[d], Quan-Zhen Li[e], M. Eric Gershwin[f], Hamid Kashkar[g], and Michel C. Nussenzweig[b,h,1]

[a]Experimental Immunology Branch, Center for Cancer Research, National Cancer Institute, National Institutes of Health, Bethesda, MD 20892; [b]Laboratory of Molecular Immunology, The Rockefeller University, New York, NY 10065; [c]Key Laboratory of Medical Molecular Virology (Ministry of Education/National Health Commission/Chinese Academy of Medical Sciences), School of Basic Medical Sciences, Shanghai Medical College, Fudan University, 20032 Shanghai, China; [d]Laboratory of Comparative Pathology, Memorial Sloan–Kettering Cancer Center, Weill Cornell Medicine, The Rockefeller University, New York, NY 10065; [e]Department of Immunology and Internal Medicine, University of Texas Southwestern Medical Center, Dallas, TX 75490; [f]Division of Rheumatology, Allergy and Clinical Immunology, University of California, Davis, CA 95616; [g]Institute for Medical Microbiology, Immunology and Hygiene, Cologne Excellence Cluster on Stress Responses in Aging-Associated Diseases Research Center, University of Cologne, 50935 Cologne, Germany; and [h]HHMI, The Rockefeller University, New York, NY 10065

Contributed by Michel C. Nussenzweig, August 23, 2020 (sent for review July 22, 2020; reviewed by Betty Diamond and Patrick C. Wilson)

B lymphocytes acquire self-reactivity as an unavoidable byproduct of antibody gene diversification in the bone marrow and in germinal centers (GCs). Autoreactive B cells emerging from the bone marrow are silenced in a series of well-defined checkpoints, but less is known about how self-reactivity that develops by somatic mutation in GCs is controlled. Here, we report the existence of an apoptosis-dependent tolerance checkpoint in post-GC B cells. Whereas defective GC B cell apoptosis has no measurable effect on autoantibody development, disruption of post-GC apoptosis results in accumulation of autoreactive memory B cells and plasma cells, antinuclear antibody production, and autoimmunity. The data presented shed light on mechanisms that regulate immune tolerance and the development of autoantibodies.

B lymphocytes | autoantibody | antinuclear antibodies | apoptosis

Landsteiner's observation that mammals can mount specific immune responses to chemically synthesized neo-antigens that do not exist in nature revealed the diversity of immune responses and brought into focus the question of how self-reactivity is avoided. Two relatively random DNA transactions generate this diversity in B lymphocytes: variable diversity and joining gene segment (V(D)J) recombination and somatic hypermutation (SHM).

Self-reactive antibodies are frequent byproducts of V(D)J recombination. They are eliminated by gene replacement, deletion, or anergy at defined checkpoints during B cell development (1–4). Like V(D)J recombination, SHM of antibody genes in germinal centers can also produce self-reactive antibodies (5, 6). Indeed, somatically mutated antibodies are implicated in the etiology of a number of different autoimmune disorders including rheumatoid arthritis and systemic lupus erythematosus (7, 8).

Two mechanisms censor autoreactive B cells that arise by mutation in germinal centers. They can be deleted by high-affinity interaction with self-antigen (9–11), or alternatively, their receptors can be revised by continued mutation and selection (12–15). Apoptosis appears to be an important regulator of self-reactive B cells that arise by mutation because inhibition of the Bcl-2–dependent pathway leads to accumulation of self-reactive antibodies and autoimmunity (16–18). However, the precise nature of the apoptosis-dependent checkpoint that silences the autoreactive B cells that arise during immune responses has not been determined. Here, we examine how apoptosis regulates the emergence of autoimmunity and define post-GC checkpoints for autoreactivity.

Results

Autoreactive GC B Cells Are Not Preferentially Undergoing Apoptosis. To document the number of autoreactive cells in GCs, we immunized apoptosis indicator mice ($Ig\kappa^{INDIA}$, $Rosa26^{INDIA}$) (19) and cloned antibodies from purified live and dying GC light zone (LZ) and dark zone (DZ) cells. Antibodies were tested for self-reactivity by immunofluorescence on HEp-2 cells (1, 6). High-affinity autoantibodies binding to HEp-2 cells at concentrations of 1 μg/mL were rarely detected in any GC compartment independent of the antigen used for immunization (*SI Appendix*, Fig. S1*A*). Even when tested at high concentrations (100 g/mL), only a small number of GC B cells expressed HEp-2–reactive antibodies with no significant accumulation of such cells in the apoptotic compartment (Fig. 1*A*) (19). Thus, autoreactive GC B cells arising in response to 4-hydroxy-3-nitrophenyl (NP)-conjugated ovalbumin (NP-OVA) or an HIV-1 envelope protein (GT1.1; ref. 19) are rare and do not accumulate in the apoptotic compartment in GCs.

The specificity of the few autoantibodies that developed in response to the two antigens differed in that the majority of the weakly autoreactive NP-specific $IgH_{V1\text{-}72}Ig\lambda$ antibodies targeted mitochondria (Fig. 1 *A* and *B* and *SI Appendix*, Fig.S1 *B* and *C*). In contrast, IgH Igκ autoantibodies produced after GT1.1/NP-OVA immunization were predominantly anti-nuclear (Fig. 1 *A* and *B* and *SI Appendix*, Fig. S1 *B* and *D*). Thus, the specificity of autoreactive antibodies produced by mutation in the GC depends in part on the antigen that initiates the response and on the immunoglobulin genes used by the responding B cells.

To determine whether disruption of apoptosis leads to accumulation of autoreactive B cells in the GC, we produced 90:10 bone

Significance

A number of autoimmune diseases feature somatically mutated self-reactive antibodies that develop in germinal centers. Defects in apoptosis are associated with autoimmunity and increased autoantibody production, suggesting that apoptosis is an important control mechanism for autoimmune antibodies. We show that some autoreactive antibodies are tolerated in GC and uncover an apoptosis-dependent tolerance checkpoint in memory B and plasma cells.

Author contributions: C.T.M., Q.W., and M.C.N. designed research; C.T.M., J.P.N., A.G., M.C., Q.W., S.M., and Q.-Z.L. performed research; A.G., M.C., M.E.G., and H.K. contributed new reagents/analytic tools; C.T.M., J.P.N., T.Y.O., V.R., S.M., and Q.-Z.L. analyzed data; and C.T.M. and M.C.N. wrote the paper.

Reviewers: B.D., Feinstein Institute for Medical Research; and P.C.W., The University of Chicago.

The authors declare no competing interest.

[1]To whom correspondence may be addressed. Email: christian.mayer@nih.gov or nussen@rockefeller.edu.

This article contains supporting information online at https://www.pnas.org/lookup/suppl/doi:10.1073/pnas.2015372117/-/DCSupplemental.

First published September 22, 2020.

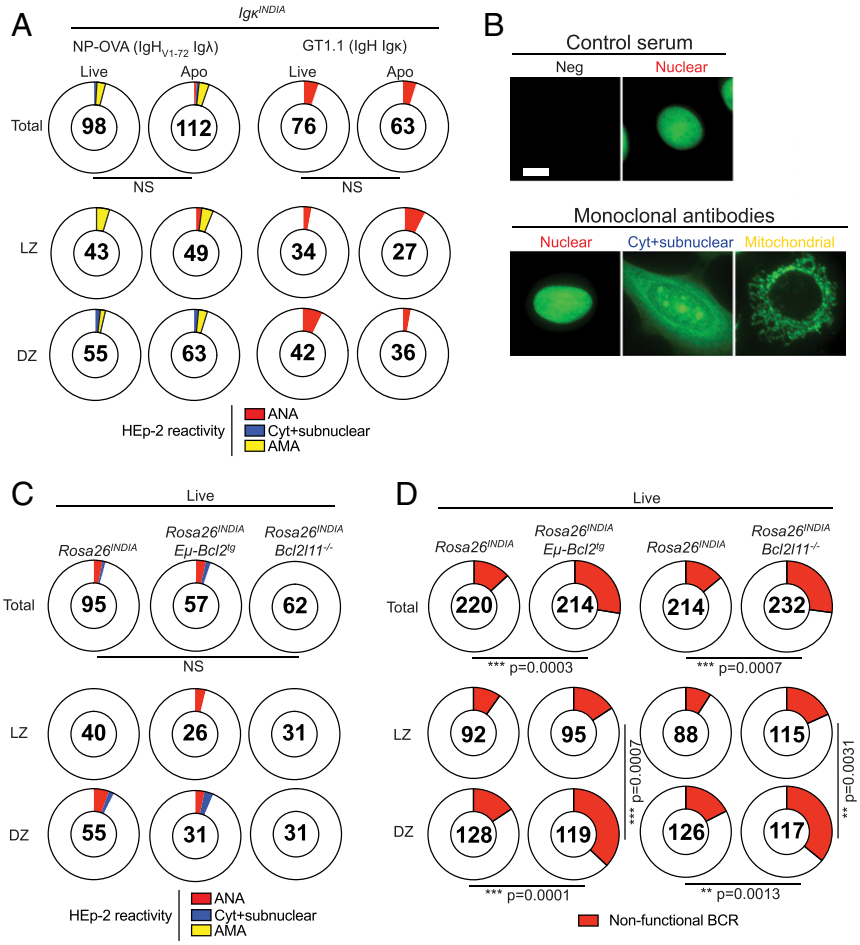

Fig. 1. Autoreactivity and apoptosis in the GC. (*A* and *B*) *Igκ*^{INDIA} mice were immunized with NP-OVA or an HIV-1 envelope protein (GT1.1) followed by single-cell sorting of FRET^{+} (live) and FRET^{-} (apoptotic) DZ and LZ GC B cells. Monoclonal antibodies were tested at 100 μg/mL for reactivity against HEp-2 cells by indirect immunofluorescence. (*A*) Pie charts show distributions of anti-nuclear (red), cytoplasmic+subnuclear (blue), and anti-mitochrondrial (yellow) autoantibodies in the indicated GC compartments after NP-OVA or GT.1.1 immunization. (*B*) Representative examples of HEp-2 fluorescence patterns. (Scale bar, 10 μm.) (*C* and *D*) Mixed bone marrow chimeras were immunized with NP-OVA. Fourteen days later, FRET^{+} (live) GC B cells of indicated donor-derived genotypes were single-cell sorted. After cDNA generation, IgH and IgL chains were amplified by PCR, sequenced, cloned, and monoclonal antibodies were produced. (*C*) Distribution of autoreactive HEp-2 cell patterns. (*D*) Distribution of nonfunctional BCRs among indicated genotypes and GC compartments. (*A*, *C*, and *D*) The number in the center of each pie chart indicates the total number of monoclonal antibodies or IgH/IgL sequence pairs assessed. Statistical significance was determined by Fisher's exact test. (*A* and *B*) For NP-OVA experiments, GC B cells of indicated compartments were single-cell sorted from pools of 1–13 mice per experiment (72 mice in total) with four to nine independent experiments per compartment and each experiment contributing between 1 and 33 antibodies per pie. For GT1.1 experiments, GC B cells of indicated compartments were single-cell sorted from pools of 7–10 mice per experiment (41 mice in total) with four to five independent experiments per compartment and each experiment contributing between 3 and 22 antibodies per pie. (*C* and *D*) For mixed bone marrow chimera experiments, GC B cells of indicated compartments and genotypes were single-cell sorted from pools of 10 mice per experiment (40 mice in total) with two to four independent experiments per compartment and each experiment contributing between 3 and 41 antibodies (*C*) or 37 and 83 sequences (*D*) per pie.

marrow chimeras consisting of *Rosa26*^{INDIA}:*Rosa26*^{INDIA}*Eμ-Bcl2*^{tg} or *Rosa26*^{INDIA}:*Rosa26*^{INDIA}*Bcl2l11*$^{-/-}$ cells (*SI Appendix*, Fig. S1*E*). Reconstituted mice were immunized with NP-OVA and antibodies cloned from live LZ and DZ B cells were tested for autoreactivity. Disrupting apoptosis did not result in accumulation of live autoreactive B cells in the GC (Fig. 1*C* and *SI Appendix*, Fig. S1*F*). As a control, we also examined the number and distribution of B cells with defective B cell receptors (*SI Appendix*, Fig. S1*G*). As expected, the proportion of live B cells with nonfunctional B cell receptors was increased by Bcl-2 overexpression or Bim (*Bcl2l11*) deletion (19) (Fig. 1*D*). Thus, the intrinsic apoptosis pathway regulates the survival of B cells that lose their receptors but has no measurable effect on the survival of autoreactive cells in the GC.

Characterization of Mouse Strains with Defective B Cell Apoptosis. Despite having little measurable effect on the survival of autoantibody-producing cells in the GC, defects in the intrinsic apoptosis pathway are associated with development of anti-nuclear antibodies and lupus-like autoimmune diseases (16–18). To pinpoint the apoptosis-dependent checkpoints for autoreactivity, we compared three strains of mice: *Eμ-Bcl2*^{tg} mice that express Bcl-2 throughout the B cell compartment (16); *Aicda*^{Cre}*Rosa26*$^{LSL\text{-}Bcl2\text{-}IRES\text{-}GFP}$ (*Aicda*^{Cre}*R26*$^{LSL\text{-}Bcl2}$; refs. 20, 21) mice where Bcl-2 overexpression begins in GC B cells and persists thereafter; *Aicda*$^{IRES\text{-}mNeonGreen\text{-}P2A\text{-}Bcl2}$ knock-in mice (*Aicda*$^{IRES\text{-}Bcl2}$, Fig. 2*A*), a strain wherein Bcl-2 expression is limited to activated and GC B cells that express *Aicda*. *Aicda* is haploinsufficient in *Aicda*^{Cre}*R26*$^{LSL\text{-}Bcl2}$ mice but intact in *Aicda*$^{IRES\text{-}Bcl2}$ mice. B cell development in the bone marrow and throughout the pre-GC stage was intact in all strains, with the exception of reduced marginal zone B cells and possible alterations of the repertoire in *Eμ-Bcl2*^{tg} mice (*SI Appendix*, Fig. S2 *A–E*) (22). However, following immunization the number of GC B cells was increased in all Bcl-2–overexpressing strains

compared to controls (Fig. 2*B*). In addition, there was an increased DZ/LZ ratio and decreased apoptosis in both DZ and LZ compartments in all three strains (Fig. 2 *C*–*F*). Similar results were obtained for chronic GCs in Peyer's patches (*SI Appendix*, Fig. S2 *F*–*J*) and for NP-OVA immunized $Aicda^{Cre}Bcl2l11^{fl/fl}$ mice (*SI Appendix*, Fig. S2 *K*–*O*). Direct comparison of aCasp3 levels in GC B cells revealed no significant differences between $E\mu\text{-}Bcl2^{tg}$ and $Aicda^{IRES\text{-}Bcl2}$ mice (*SI Appendix*, Fig. S2*P*), suggesting similar functional levels of Bcl-2 expression. aCasp3 levels were lower in $Aicda^{Cre}R26^{LSL\text{-}Bcl2}$ mice (*SI Appendix*, Fig. S2*P*).

We compared green fluorescent reporter expression as a surrogate for knock-in gene activity in $Aicda^{Cre}R26^{LSL\text{-}Bcl2}$ and $Aicda^{IRES\text{-}Bcl2}$ mice. As expected, green fluorescence was present in GCs but extinguished in $Aicda^{IRES\text{-}Bcl2}$ post-GC B cells, while it persisted in $Aicda^{Cre}R26^{LSL\text{-}Bcl2}$ memory B cells (MBCs) and plasma cells (PCs; Fig. 2*G*). Persistent Bcl-2 expression in PCs and MBCs in $Aicda^{Cre}R26^{LSL\text{-}Bcl2}$ mice was associated with significantly increased numbers of these cells (Fig. 2*H*). Similar effects were also seen in $Aicda^{Cre}Bcl2l11^{fl/fl}$ mice (*SI Appendix*, Fig.S2 *Q* and *R*). In contrast, PC and MBC compartments were indistinguishable from control in $Aicda^{IRES\text{-}Bcl2}$ mice (Fig. 2*H*). We conclude that $Aicda^{Cre}R26^{LSL\text{-}Bcl2}$ interferes with apoptosis in GC and post-GC compartments, whereas the effects of $Aicda^{IRES\text{-}Bcl2}$ appear to be limited to the GC.

A Post-GC Tolerance Checkpoint for Autoimmunity. To examine the roles of GC and post-GC B cell apoptosis in censoring autoreactive antibody development, we aged $E\mu\text{-}Bcl2^{tg}$, $Aicda^{Cre}R26^{LSL\text{-}Bcl2}$ and $Aicda^{IRES\text{-}Bcl2}$ mice, as well as $Bcl2l11^{-/-}$ positive control mice, and tested their serum for IgG reactivity against HEp-2 cells. As expected, $E\mu\text{-}Bcl2^{tg}$ and $Bcl2l11^{-/-}$ mice rapidly developed serologic self-reactivity, and by 36 wk most of the mice had high titers of antinuclear antibodies (Fig. 3 *A* and *B*, $P < 0.0001$, and *SI Appendix*, Fig. S3*A*). Despite *Aicda* haploinsufficiency, similar results were observed in $Aicda^{Cre}R26^{LSL\text{-}Bcl2}$ mice wherein Bcl-2 over-expression is limited to the GC and to post-GC B cells. In contrast, *Aicda* sufficient $Aicda^{IRES\text{-}Bcl2}$ mice were indistinguishable from controls throughout the observation period (Fig. 3 *A* and *B*). The presence of serum IgG autoantibodies was confirmed by autoantigen arrays showing stronger reactivity in $E\mu\text{-}Bcl2^{tg}$ and $Aicda^{Cre}R26^{LSL\text{-}Bcl2}$ compared with $Aicda^{IRES\text{-}Bcl2}$ mice (*SI Appendix*, Fig. S3*B* and Dataset S1). Autoantibodies were also detected in 28-wk-old $Aicda^{Cre}Bcl2l11^{fl/fl}$ mice (*SI Appendix*, Fig. S3*C*) in which the effects on GC B cell apoptosis are lower than in $Aicda^{IRES\text{-}Bcl2}$ mice.

To examine which post-GC B cell compartment censors autoreactive B cells by apoptosis, we purified single bone marrow and spleen PCs (BMPCs and SpPCs) and used double-stranded DNA (dsDNA) to enrich self-reactive MBCs. IgG antibodies were cloned, expressed, and tested for reactivity against HEp-2 cells. Although the number of cells examined was limited, autoreactivity was only detected in SpPCs and MBCs (Fig. 3*C* and *SI Appendix*, Fig. S3 *D*–*H*). Autoreactive antibodies, including two clones with shared IgHV1-26/IgκV4-74 genes, were found in $E\mu\text{-}Bcl2^{tg}$ and $Aicda^{Cre}R26^{LSL\text{-}Bcl2}$ mice, but not in WT or $Aicda^{IRES\text{-}Bcl2}$ mice (Fig. 3*C* and Dataset S2).

Since the number of cells that can be interrogated by antibody cloning is limited, we also performed nucleosome-specific ELISpot assays on IgG^+ MBCs, SpPCs, and BMPCs. Consistent with the cloning results, we found increased numbers of nucleosome reactive MBCs and SpPCs in $E\mu\text{-}Bcl2^{tg}$ and $Aicda^{Cre}R26^{LSL\text{-}Bcl2}$ mice (Fig. 3 *D* and *E*). Moreover, this reactivity was not detectable in WT and $Aicda^{IRES\text{-}Bcl2}$ mice. The proportion of nucleosome-reactive MBCs and SpPCs found by ELISpot in $E\mu\text{-}Bcl2^{tg}$ and $Aicda^{Cre}R26^{LSL\text{-}Bcl2}$ mice (MBCs: 0.7% and 1.4%; SpPC: 1.6% and 9.3%) was similar to that obtained by antibody cloning.

Antibodies cloned from autoreactive SpPCs and MBCs showed features associated with autoreactivity (1, 5) including long IgH

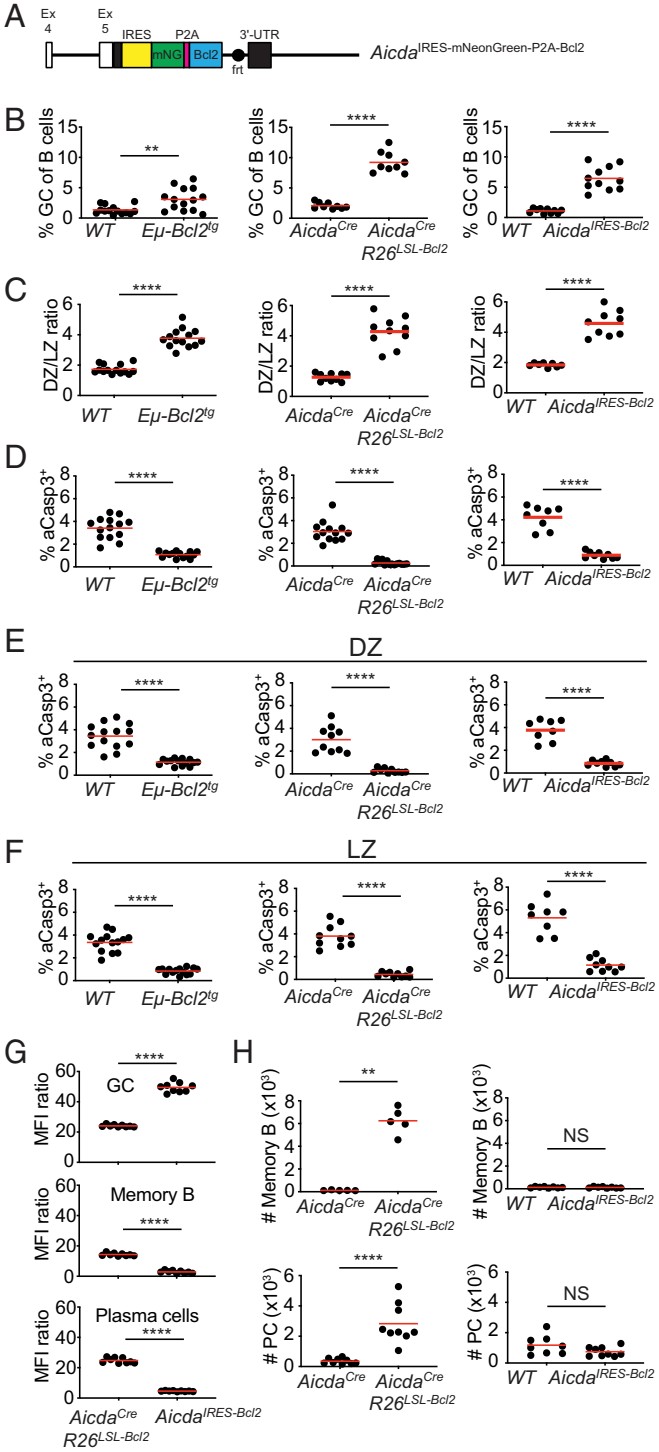

Fig. 2. GC-restricted apoptosis inhibition in $Aicda^{IRES\text{-}Bcl2}$ mice. (*A*) Schematic of the targeted locus in $Aicda^{IRES\text{-}mNeonGreen\text{-}P2A\text{-}mBcl2}$ ($Aicda^{IRES\text{-}Bcl2}$) knock-in mice. (*B*–*H*) $E\mu\text{-}Bcl2^{tg}$, $Aicda^{Cre}Rosa26^{LSL\text{-}Bcl2\text{-}IRES\text{-}GFP}$ ($Aicda^{Cre}R26^{LSL\text{-}Bcl2}$), $Aicda^{IRES\text{-}Bcl2}$, and control mice were immunized subcutaneously with NP-OVA. Fourteen days later, draining lymph nodes were analyzed by flow cytometry. (*B*) Fraction of $CD38^-Fas^+$ GC B cells among $CD19^+$ B cells. (*C*) Ratio of DZ ($CXCR4^{hi}CD86^{lo}$) to LZ ($CXCR4^{lo}CD86^{hi}$) GC B cells. (*D*–*F*) Fraction of $aCasp3^+$ cells among total GC B cells (*D*), or DZ (*E*) and LZ (*F*) GC B cells. (*G*) Green mean fluorescence intensity ratio of indicated genotypes over control $CD19^+CD38^-Fas^+$ GC B cells, $CD19^+IgG1^+CD38^+Fas^{lo}$ MBCs, and $CD19^{+/lo}CD138^{hi}$ Peyer's patch plasma cells (PCs). (*H*) Numbers of MBCs and PCs. (*B*–*H*) Results are from at least two independent experiments. $^{**}P = 0.006$ (*B*), $^{**}P = 0.008$ (*H*), $^{****}P < 0.0001$ (Mann–Whitney test).

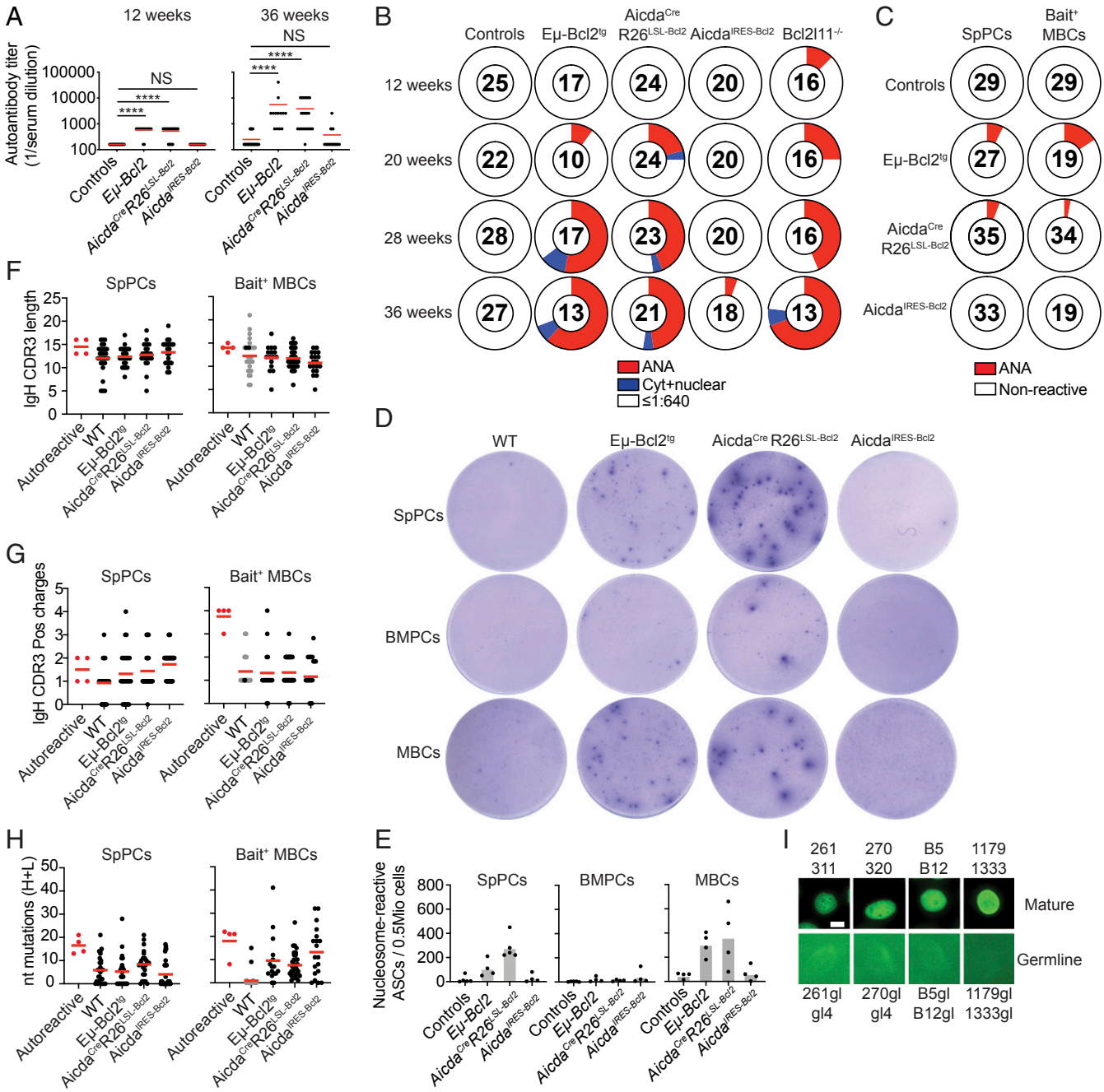

Fig. 3. Apoptosis censors self-reactive plasma cells and MBCs. Cohorts of Eμ-Bcl2^{tg}, *Aicda*^{Cre}*R26*$^{LSL\text{-}Bcl2}$, *Aicda*$^{IRES\text{-}Bcl2}$, and control mice were monitored over time. (*A*) End titers of serum HEp-2 cell reactivity at 12 or 36 wk. Serum was assessed starting at a 1:640 and consecutive fourfold dilutions. Negative reactivity is shown as 1:160. ****$P < 0.0001$ (Kruskall–Wallis test). (*B*) HEp-2 cell patterns of high titer (≥1:2,560) autoantibodies. Anti-nuclear reactivity (red), cytoplasmic and nuclear staining (blue), and nonreactive (white) are shown. Numbers in the centers of each pie chart represent the total number of mice assessed. (*C*) Reactivity against HEp-2 cells by spleen PC (SpPC) or DNA-bait enriched MBC antibodies. Pie charts summarize HEp-2 cell reactivity. Antinuclear reactivity assayed at 1 μg/mL (red). The number in the center of each pie represents the total number of antibodies tested. Individual mice were sorted with two to three independent experiments performed per compartment and each experiment contributing between 3 and 25 antibodies per pie. (*D* and *E*) SpPCs, BMPCs, and activated MBCs were assayed for nucleosome reactivity by ELISpot. (*D*) Representative images display spots for each genotype after the addition of 50,000 total cells, except for WT and *Aicda*$^{IRES\text{-}Bcl2}$ MBCs where the input was 75,000 and 175,000, respectively. (*E*) Quantitation of nucleosome-specific antibody-secreting cells (ASCs) per 0.5 million input cells. (*F–H*) Graphs summarize lengths of the IgH CDR3s (*F*) and the number of positively charged amino acids in the IgH CDR3s (*G*) and number of nucleotide mutations in IgH and IgL chains (*H*) in autoreactive (red dots) and nonautoreactive antibodies cloned from cells from the indicated genotypes. All IgH sequences amplified were of IgG isotype (black dots) except for WT dsDNA bait^{+} MBCs for which only two IgG sequences were obtained, and IgM sequences were amplified (gray dots). (*I*) HEp-2 cell patterns of indicated autoreactive monoclonal antibodies and their respective germ-line versions. (Scale bar, 10 μm.) Results are from at least three independent cohorts of mice. Two mice per genotype were single-cell sorted. (*D* and *E*) Two independent experiments were combined.

CDR3s enriched in positively charged amino acids (Fig. 3 *F* and *G*). In addition, these antibodies were somatically mutated (Fig. 3*H*). To determine if the somatic mutations contributed to antibody self-reactvity, we reverted the antibodies to their inferred germ-line configuration. Four of five germ-line antibodies completely lost autoreactivity, including IgHV1-26/IgκV4-74

antibodies (Fig. 3*I* and Dataset S2) (5). The fifth germ-line antibody corresponding to an IgHV1-26/IgκV4-74 clone with three members was autoreactive in its germ-line configuration (*SI Appendix*, Fig. S3*I*). In summary, B cells that became autoreactive in GCs and/or escaped pre-GC checkpoints are censored by apoptosis in MBC and PC compartments.

To determine if post-GC apoptosis-dependent checkpoints contribute to disease development, we aged cohorts of *Bcl2l11*$^{-/-}$, *Eμ-Bcl2*^{tg}, *Aicda*^{Cre}*R26*$^{LSL\text{-}Bcl2}$, *Aicda*$^{IRES\text{-}Bcl2}$, and control mice (Fig. 4*A*). *Bcl2l11*$^{-/-}$, *Eμ-Bcl2*^{tg}, and *Aicda*^{Cre}*R26*$^{LSL\text{-}Bcl2}$ showed early mortality that was associated with glomerulonephritis or B cell lymphoma, whereas *Aicda*$^{IRES\text{-}Bcl2}$ and control mice did not (Fig. 4 *A*–*D*, *SI Appendix*, Fig. S4*A*, and Dataset S3) (16, 17). The lymphomas were associated with ascites and expression of PC markers as expected for apoptosis defects in the PC compartment of *Bcl2l11*$^{-/-}$, *Eμ-Bcl2*^{tg}, and *Aicda*^{Cre}*R26*$^{LSL\text{-}Bcl2}$ mice (*SI Appendix*, Fig. S4 *B* and *C*). Finally, disease development was more prominent in *Bcl2l11*$^{-/-}$ and *Eμ-Bcl2*^{tg} mice where apoptosis is defective throughout the B cell pathway and not limited to GCs and post-GC compartments.

Discussion

Self-reactivity is an unavoidable byproduct of random antigen receptor diversification that must be eliminated to avoid autoantibody production and autoimmunity. For example, over 50% of the antibodies produced by V(D)J recombination are autoreactive (1). These antibodies are removed from the B cell repertoire by deletion (3), receptor editing (4), or anergy (2), leaving only a small number of such cells with very low affinity polyreactive receptors in the naïve B cell compartment (1).

Highly autoreactive B cells that develop in the GC are subject to deletion (9–11). These cells are not enriched in the apoptotic compartment in GCs, suggesting that they are either very rare or that apoptosis does not play an important role in B cell deletion in the GC. Autoreactive GC antibodies can also be replaced by receptor revision, which is mediated by persistent mutation (12–15). Our experiments indicate that autoreactive B cells are rare in GCs and that they are not regulated by apoptosis. One possible explanation is that the antigens necessary for B cell deletion are not available at sufficiently high concentrations in the GC for most self-reactive B cells arising in this compartment and/or that the strength of BCR signaling in GC B cells is not sufficient to trigger cell death. The data are consistent with the observation that GCs tolerate higher levels of polyreactivity than naïve B cells as evidenced by an increase in the number of polyreactive cells in the GC and their subsequent removal from the MBC compartment (6, 23).

Among the tolerance mechanisms that censor autoreactivity in the GC or post-GC compartments, only apoptosis and receptor revision have been linked to disease development (12, 16–18). Our experiments indicate that self-reactive antibodies that escape deletion and receptor revision in the GC are eliminated by apoptosis in MBCs and SpPCs. This mechanism is essential to avert persistence of post-GC autoantibody production and autoimmunity.

Materials and Methods

Mice. B6.Cg-Tg(ACTFLPe)9205Dym/J, B6.129S1-Bcl2l11tm1.1Ast/J (*Bcl2l11*$^{-/-}$), B6.129P2-Aicdatm1(cre)Mnz/J (*Aicda*^{Cre}), B6(Cg)-Tyr^{c-2J}/J, B6.SJL, and C57BL/6J mice were purchased from Jackson Laboratories. *Igκ*^{INDIA} *and Rosa26*^{INDIA} mice were previously described (19). *Rosa26*$^{LSL\text{-}Bcl2\text{-}IRES\text{-}GFP}$ mice (20, 21) were crossed with Aicda^{Cre}. Eμ-Bcl2-22^{tg} mice (16) were backcrossed to C57BL/6J for at least 10 generations. *Bcl2l11*$^{fl/fl}$ mice (18) were kindly provided by S. Katz (Yale School of Medicine, New Haven, CT) and backcrossed to B6 for at least eight generations. Bone marrow chimeras were generated as described (24). All animal experiments were approved by the Institutional Review Board and the Institutional Animal Care and Use Committee at The Rockefeller University.

Aicda$^{IRES\text{-}Bcl2}$ Mice. A 3,734-bp DNA sequence consisting of flanking restriction sites, an internal ribosomal entry site (IRES) from encephalomyocarditis virus, a fusion protein composed of sequence optimized N-terminally Myc-tagged mNeonGreen (19, 25), a self-cleaving P2A sequence (GSGATNFSLLKQAGDVEENPGP), and mouse *Bcl2* complementary DNA (cDNA) (NM_009741.5), followed by a FRT-flanked Neo resistance cassette, was synthesized by Genescript. A pBluescript-based targeting vector containing a DTA negative selectable marker, 2,002-bp 5′- and 1,303-bp 3′ homology arms, and the *IRES-mNeonGreen-P2A-Bcl2-frt-Neo-frt* cassette was constructed using PCR and standard cloning procedures. To generate *Aicda*$^{IRES\text{-}mNeonGreen\text{-}P2A\text{-}Bcl2\text{-}frt\text{-}Neo\text{-}frt}$ knock-in mice, DNA double-strand breaks were generated in the 3′ untranslated region of the *Aicda* locus in CY2.4 albino C57BL/6J-Tyr^{c-2J}-derived ES cells by CRISPR/Cas9 (sgRNA sequence: CCAGAGCAATGATGTAACTGAGC) followed by homology-directed repair with the targeting vector (Gene Targeting Resource Center, The Rockefeller University). Correct *Aicda* modification was verified by Southern blot and PCR. Chimeric males obtained after blastocyst injection were crossed to B6(Cg)-Tyr^{c-2J}/J females that also ubiquitously expressed Flpe. *Aicda*$^{IRES\text{-}mNeonGreen\text{-}P2A\text{-}Bcl2}$ (*Aicda*$^{IRES\text{-}Bcl2}$ mice) exhibiting germ-line transmission and concomitant deletion of the Neo cassette were identified by coat color and PCR and were then crossed to C57BL/6J. *Aicda*$^{IRES\text{-}Bcl2}$ offspring that lost Flpe were used for further breeding. Genotyping was performed by PCR on tail DNA.

Immunizations and Treatments. Primary GCs were elicited by immunizing mice of the indicated genotypes s.c. with 25 μL of PBS containing 12.5 μg of NP_{15}-OVA or NP_{20}-OVA (Biosearch Technologies) or 4 μg of HIV envelope antigen (BG505 SOSIP.v4.1-GT1.1 trimers, GT1.1) (19) precipitated in alum (Imject alum, ThermoFisher Scientific) at a 2:1 ratio. In case of NP-OVA immunization for single-cell sorting, mice were also immunized intraperitoneally with

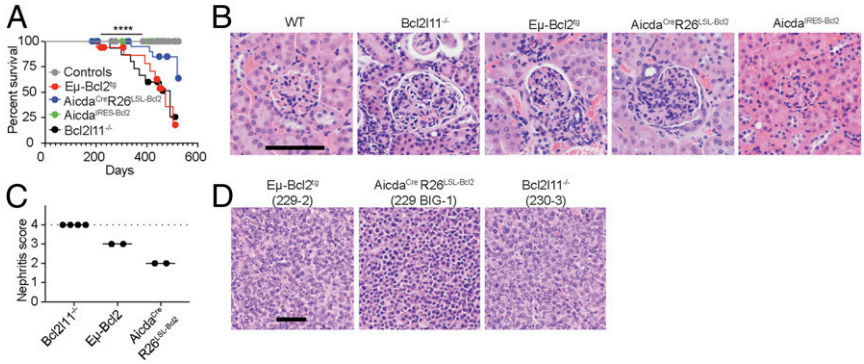

Fig. 4. Post-GC B cell apoptosis prevents disease. (*A*) Kaplan–Meyer plot showing survival (Controls, $n = 32$; Eμ-Bcl2^{tg}, $n = 17$; *Aicda*^{Cre}*R26*$^{LSL\text{-}Bcl2}$, $n = 24$; *Aicda*$^{IRES\text{-}Bcl2}$, $n = 20$). ****$P < 0.0001$ (log-rank Mantel–Cox test). (*B* and *C*) Formalin-fixed H&E stained kidney sections. (*B*) Representative micrographs depict glomerular pathology for indicated genotypes. (*C*) Blinded quantitation of glomerulonephritis among diseased mice. (*D*) H&E-stained intestinal tumor biopsies from terminally diseased mice. Results are combined from at least three independent cohorts of mice. (Scale bars, *B*, 100 μm; *D*, 50 μm.)

100 μL of PBS containing 50 μg of NP_{15}-OVA or NP_{20}-OVA precipitated in alum.

Bait Preparations. A 5′ biotinylated forward primer (/5Biosg/GGA CCC AAC-CCA GGA GGC AGA TGT) and an unmodified reverse primer (CCT CTA AGG-CTT CGC TGT TAT TAC CAC) were used to amplify a 500-bp DNA fragment from mouse genomic DNA using Taq DNA polymerase (Qiagen). The 500-bp fragment was purified by agarose gel electrophoresis followed by extraction from the gel. The DNA concentration was determined by Nanodrop, and integrity was verified by agarose gel electrophoresis. To generate an irrelevant protein bait, ovalbumin (Sigma) was biotinylated with the EZ-Link Micro NHS-PEG4-Biotinylation Kit (Thermo Fisher) according to the manufacturer's instructions. Prior to B cell staining, each biotinylated bait was adjusted to 250 nM in PBS and mixed with fluorochrome-conjugated streptavidin at a 5:1 molar ratio. After incubation for 30 min at 4 °C, B cells were stained at 30 nM per fluorochrome-conjugated bait.

Single-Cell Sorting. Enrichment and single-cell sorting of $Igκ^{INDIA}$ GC B cells were performed as described (19). For NP-OVA–immunized mixed bone marrow chimeras, $Rosa26^{INDIA}$ GC B cells were enriched similarly but identified as $B220^+$DUMP(CD4,CD8,NK1.1,F4/80)$^-Fas^+CD38^-$mRuby2$^+$. Live ($FRET^+$) LZ ($CXCR4^{lo}CD86^{hi}$) and DZ ($CXCR4^{hi}CD86^{lo}$) GC B cells were single-cell sorted. Different genotypes in the mixed chimeras were identified by staining for CD45.1 and CD45.2.

Plasma cells were single-cell sorted from bone marrow or spleen, and MBCs were sorted from spleens of aged untreated mice (>200 d old) of indicated genotypes. Plasma cells were gated as $CD138^{hi}$DUMP(CD4, CD8, NK1.1, F4/80)$^-B220^{-/lo}$ cells. MBCs were gated as $CD19^+$DUMP(CD4, CD8, NK1.1, F4/80)$^-IgM^-IgD^-Fas^-CD38^+$ cells. For dsDNA bait sorting, $B220^+$DUMP(CD4, CD8, NK1.1, F4/80)$^-$ B cells that did not bind to OVA-PECy7 but to dsDNA-Alexa647 and to dsDNA-BV421 were single-cell sorted.

Single-cell sorting was carried out on a FACS Aria II (BD Biosciences). Single cells were sorted into 96-well PCR plates containing 4 μL of lysis buffer (26) and were either directly processed or stored at −80 °C.

Flow Cytometry. Single-cell suspensions were prepared and stained as described (19). α-CD4 (rat mAb RM4-5), α-CD8α (rat mAb 53–6.7), α-CD19 (rat mAb eBio1D3), α-CD38 (rat mAb 90), α-CD45R/B220 (rat mAb RA3-6B2), α-CD93 (rat mAb AA4.1), α-F4/80 (rat mAb BM8), α-GL7 (rat mAb GL7), α-IgM (rat mAb II/41), and α-NK1.1 (mouse mAb PK136) were from Thermo Fisher Scientific. α-CD19 (rat mAb 6D5), α-CD23 (rat mAb B3B4), α-CD25 (rat mAb PC61), α-CD45.2 (mouse mAb 104), and α-CD138 (281-2) were from BioLegend. α-aCasp3 (Alexa Fluor 647-conjugated; rabbit mAb C92-605), α-CD19 (rat mAb 1D3), α-CD21/CD35 (rat mAb 7G6), α-CD43 (rat mAb S7), α-CD45.1 (mouse mAb A20), α-CD86 (rat mAb GL1), α-CXCR4 (rat mAb 2B11), α-Fas (hamster mAb Jo2), α-IgD (rat mAb 11–26c.2a), α-Igκ (rat mAb 187.1), α-$Igλ_{1-3}$ (rat mAb R26-46), α-IgG1 (rat mAb A85-1), streptavidin conjugated to V500, and α-T and B cell activation antigen (rat mAb GL7) were from BD Biosciences. Dead cells were excluded by staining with Zombie-NIR (BioLegend), or by adding DAPI (Sigma, 0.04 μg/mL) or propidium iodide (0.04 μg/mL) prior to acquisition.

Flow cytometry data were acquired on a BD Fortessa (BD Biosciences), and data were analyzed with Flowjo (Tristar). Intact cells and singlets were identified by their FSC-A/SSC-A and SSC-A/SSC-W profiles, by lack of staining with dead cell dyes and, in the case of $Igκ^{INDIA}$ and $Rosa26^{INDIA}$ B cells, additionally by mRuby2 expression. For analysis of B cell development, the following subsets were identified in the bone marrow: prepro B ($B220^+CD43^+CD19^-IgM^-$), pre-BI ($B220^+CD43^+CD19^+IgM^-CD25^-IgD^-$), pre-BII ($B220^+CD43^-IgM^-CD25^+$), immature B cells ($B220^+CD43^-IgM^+CD25^-IgD^-$), recirculating B cells ($B220^{hi}IgM^+CD19^+IgD^+$). In the spleens, the following subsets were gated: Transitional B cells (T1, $CD19^+B220^+CD93^+IgM^+CD23^{lo}$; T2, $CD19^+B220^+CD93^+IgM^+CD23^+$; T3, $CD19^+B220^+CD93^+IgM^{lo}CD23^+$), marginal zone B cells ($CD19^+B220^+CD93^-IgM^{hi}CD21/CD35^+$), follicular B cells ($CD19^+B220^+CD93^-CD21/CD35^-IgD^+CD23^+$). For other experiments, gating was done as indicated.

Single-Cell Cloning and Recombinant Antibody Expression. Reverse transcription, nested PCR amplification, sequencing, and ligation-independent cloning of *IgG*, *IgM*, Igλ, and Igκ, were performed as described (19). For NP-immunized mice, either $IgH_{V1\text{-}72}$ Igλ sequences or all IgH/IgL combinations were cloned as indicated. For plasma cells and MBCs, IgG subtype coverage was optimized by adding an IgG3 reverse primer (AGACTGTGCGCACACCGC-TGGAC) to the first PCR. Sequences were analyzed with IMGT/V-QUEST and IgBlast. Some *Ig* sequences were directly synthesized for cloning (IDT). *Ig* sequences were cloned into human IgG1, human Igλ, and human Igκ expression vectors, and monoclonal antibodies were expressed by transient transfection of HEK293-6E cells and purified with Protein G Sepharose 4 Fast Flow (GE Healthcare) as described (26).

HEp-2 Cell Immunofluorescence. Autoreactivity of monoclonal antibodies was assessed using the Antinuclear Antibody (HEp-2) Kit (MBL) according to the manufacturer's instructions. Antibodies were tested at 100 μg/mL or at 1 μg/mL as indicated. Autoreactivity of mouse serum was assessed using Antinuclear Antibody (HEp-2) Antigen substrate slides (MBL). Each well was incubated with a 1:640 serum dilution in phosphate-buffered saline (PBS) for 30 min at room temperature. Following two washes in PBS, wells were incubated with 10 μg/mL Alexa Fluor 488-conjugated F(ab')2 fragments of goat anti-mouse IgG(H+L) antibody (Thermo Fisher, catalog no. A11017), followed by washing and mounting of the slide. Fluorescence images from up to three different fields were acquired with an Axioplan 2 imaging upright microscope (Zeiss), a 40x dry objective, a Spot Insight QE color digital camera (700-ms exposure), and MetaVue software (Molecular Devices). Images were analyzed with ImageJ. The fluorescence intensities of five random cells per field were averaged, and the signal to background ratio was calculated. A monoclonal antibody or serum sample was considered autoreactive when the signal to background ratio exceeded 1.5 and displayed a nuclear, cytoplasmic + (sub)nuclear, or antimitochondrial fluorescence pattern. Positive reference serum and a negative control were included in each measurement. If a serum sample tested positive at the initial 1:640 dilution, serial 1:4 dilutions were performed in PBS until a negative result was obtained. The dilution that still produced a positive result was considered the end titer.

Nucleosome-Specific ELISpot. Polyvinylidene fluoride (PVDF) membranes of $MultiScreen_{HTS}$ IP filter plates (Milipore Sigma) were treated for 1 min with 35% ethanol, followed by washing with PBS. Polynucleomes (Epicypher) were coated at 12.5 μg/mL overnight at 4 °C or for 4 h at 37 °C. After washing, wells were blocked with PBS containing 2% bovine serum albumin (BSA). Spleen and bone marrow single-cell suspensions were counted by flow cytometry using AccuCheck counting beads (Life Technologies), adjusted, and plated in Freestyle293 medium for 4 h at 37 °C at different dilutions. IgG^+ MBCs were enriched from splenocytes using biotinylated antibodies to IgD, IgM, and GL7, combined with the EasySep Mouse Pan-B cell isolation kit (Stemcell Technologies) according to the manufacturer's instructions. One to five Mio cells were cultured for 2 d at 37 °C in RPMI 1640 supplemented with 10% fetal bovine serum, 1 μg/mL R848 (Invivogen), 10 ng/mL recombinant mouse IL-2 (R&D Systems), and for some experiments additionally with 0.5 μg/mL anti-CD180 (RP105, BD Biosciences). Activated cells were then washed with PBS, counted, and resuspended in Freestyle293 medium prior to culture in $MultiScreen_{HTS}$ IP filter plates as detailed above. After antibody secretion, cells were washed away with PBS 0.05% Tween 20 and IgG spots were visualized using biotinylated goat anti-mouse IgG (Southern Biotech), alkaline phosphatase-conjugated streptavidin (MabTech), and BCIP/NBT-plus substrate (MabTech). Plates were scanned on an Immunospot analyzer (CTL). Nucleosome-specific spots were counted, and the number of spots per 0.5 Mio input cells was calculated.

Autoantigen Arrays. Autoantigen arrays were performed at the Genomic and Microarray Core Facility of the University of Texas Southwestern Medical Center. In brief, 16-pad nitrocellulose film slides (Grace BioLabs) printed with 122 autoantigens or control proteins were incubated with DNase I-treated mouse serum samples at 1:50 dilutions or PBS. The antibodies bound to the antigens on the array were detected with Cyanine3-conjugated goat anti-mouse IgG(H+L) (Jackson ImmunoResearch) and a GenePix 4400A Microarray Scanner. Images were analyzed with Genepix Pro-7.0 software. The net fluorescent intensity (NFI) of each antigen was obtained by subtracting the local background and PBS control. The signal-to-noise ratio (SNR) was also calculated for each antigen. To avoid outliers in either NFI or SNR, autoantibody score (Ab-score; $\log_2$ ((NFI x SNR)+1) was used for downstream analysis. Ab scores were clustered and visualized as heatmaps using R.

Enzyme-Linked Immunosorbent Assay (ELISA). To assess anti-mitochondrial reactivity, pML-MIT3 antigen (27) was coated onto high-binding 96-well plates (Corning) at 10 μg/mL PBS. After washing with PBS containing 0.05% Tween 20 (Sigma), wells were blocked with PBS containing 1% BSA for 2 h at room temperature. Monoclonal antibodies were incubated at 100 μg/mL or seven consecutive 1:4 dilutions in PBS for 2 h at room temperature. After washing, horseradish peroxidase (HRP)-conjugated goat α-human IgG (Jackson ImmunoResearch) was added at 0.16 μg/mL for 1 h at room temperature. After additional washing, HRP was revealed with 1-Step ABTS

Substrate Solution (ThermoFisher Scientific). Absorbance was measured at 405 nm after incubation for 20 min at room temperature.

Pathology. Entire kidneys and tumors were fixed in 10% neutral buffered formalin, processed in ethanol and xylene, embedded in paraffin, sectioned at 5-microns thickness, and stained with hematoxylin and eosin (H&E). Tumors were diagnosed and glomerulonephritis was assessed in a blinded fashion by a board-certified veterinary pathologist (S.M.). A glomerulonephritis score representing the severity of pathological findings was assigned (0: normal glomeruli; 1: minimal glomerulonephritis; 2: mild glomerulonephritis; 3: moderate glomerulonephritis; 4: marked glomerulonephritis). Representative images were taken using a BX61 microscrope, DP80 camera, and cellSens Dimension software (Olympus America), using a 20× objective.

Serum urea concentrations were determined with the Urea Nitrogen (BUN) Colorimetric Detection Kit (ThermoFisher Scientific) according to the manufacturer's instructions.

Statistical Analyses. Statistical significance was determined with GraphPad Prism Version 6.0. For pie charts, statistical significance was assessed by Fisher's exact test. For group comparisons, normality was first assessed by the D'Agostino & Pearson test. If the data were normally distributed, a two-tailed Student's *t* test was used. If significant differences were detected by the normality test, a two-tailed Mann–Whitney test was used. For comparisons of more than two groups, Kruskall–Wallis test with Dunn's multiple comparisons test were used. For analysis of survival curves, a log-rank (Mantel–Cox) test was used.

Data Availability. All study data are included in the article and supporting information.

ACKNOWLEDGMENTS. We thank Thomas Eisenreich for help with mouse colony management; Daniel Yost for antibody production; Kai-Hui Yao for technical help; Kalsang Chhosphel and Kristie Gordon for cell sorting; Davide Robbiani, Mila Jankovic, Harald Hartweger, and Julia Merkenschlager, and all members of the M.C.N. laboratory for discussion. We further thank Dr. Chingwen Yang, the Gene Targeting Resource Center, and Drs. Alison North and Christina Pyrgaki from the Bio-imaging Resource Center of The Rockefeller University. This work was supported by NIH Grant 5R37 AI037526 and NIH Center for HIV/AIDS Vaccine Immunology and Immunogen Discovery Grant 1UM1AI144462-01 (to M.C.N.), and by the German Research Foundation SFB-1403–414786233 (to H.K.). M.C.N. is a HHMI Investigator. S.M. and the Laboratory of Comparative Pathology were supported in part by National Cancer Institute Grant P30 CA008748. The Bio-imaging Resource Center of The Rockefeller University was supported by the Empire State Stem Cell Fund through New York State Department of Health Contract C023046. Opinions expressed here are solely those of the author and do not necessarily reflect those of the Empire State Stem Cell Fund, the NYSDOH, or the State of New York.

1. H. Wardemann *et al*., Predominant autoantibody production by early human B cell precursors. *Science* **301**, 1374–1377 (2003).
2. C. C. Goodnow *et al*., Altered immunoglobulin expression and functional silencing of self-reactive B lymphocytes in transgenic mice. *Nature* **334**, 676–682 (1988).
3. D. A. Nemazee, K. Bürki, Clonal deletion of B lymphocytes in a transgenic mouse bearing anti-MHC class I antibody genes. *Nature* **337**, 562–566 (1989).
4. S. L. Tiegs, D. M. Russell, D. Nemazee, Receptor editing in self-reactive bone marrow B cells. *J. Exp. Med.* **177**, 1009–1020 (1993).
5. W. Guo *et al*., Somatic hypermutation as a generator of antinuclear antibodies in a murine model of systemic autoimmunity. *J. Exp. Med.* **207**, 2225–2237 (2010).
6. T. Tiller *et al*., Autoreactivity in human IgG+ memory B cells. *Immunity* **26**, 205–213 (2007).
7. B. Mietzner *et al*., Autoreactive IgG memory antibodies in patients with systemic lupus erythematosus arise from nonreactive and polyreactive precursors. *Proc. Natl. Acad. Sci. U.S.A.* **105**, 9727–9732 (2008).
8. J. Steen *et al*., Recognition of amino acid motifs, rather than specific proteins, by human plasma cell-derived monoclonal antibodies to posttranslationally modified proteins in rheumatoid arthritis. *Arthritis Rheumatol.* **71**, 196–209 (2019).
9. T. D. Chan *et al*., Elimination of germinal-center-derived self-reactive B cells is governed by the location and concentration of self-antigen. *Immunity* **37**, 893–904 (2012).
10. B. Pulendran, G. Kannourakis, S. Nouri, K. G. Smith, G. J. Nossal, Soluble antigen can cause enhanced apoptosis of germinal-centre B cells. *Nature* **375**, 331–334 (1995).
11. K. M. Shokat, C. C. Goodnow, Antigen-induced B-cell death and elimination during germinal-centre immune responses. *Nature* **375**, 334–338 (1995).
12. J. H. Reed, J. Jackson, D. Christ, C. C. Goodnow, Clonal redemption of autoantibodies by somatic hypermutation away from self-reactivity during human immunization. *J. Exp. Med.* **213**, 1255–1265 (2016).
13. Z. Sabouri *et al*., Redemption of autoantibodies on anergic B cells by variable-region glycosylation and mutation away from self-reactivity. *Proc. Natl. Acad. Sci. U.S.A.* **111**, E2567–E2575 (2014).
14. J. Tan *et al*., A LAIR1 insertion generates broadly reactive antibodies against malaria variant antigens. *Nature* **529**, 105–109 (2016).
15. D. L. Burnett *et al*., Germinal center antibody mutation trajectories are determined by rapid self/foreign discrimination. *Science* **360**, 223–226 (2018).
16. A. Strasser *et al*., Enforced BCL2 expression in B-lymphoid cells prolongs antibody responses and elicits autoimmune disease. *Proc. Natl. Acad. Sci. U.S.A.* **88**, 8661–8665 (1991).
17. P. Bouillet *et al*., Proapoptotic Bcl-2 relative Bim required for certain apoptotic responses, leukocyte homeostasis, and to preclude autoimmunity. *Science* **286**, 1735–1738 (1999).
18. O. Takeuchi *et al*., Essential role of BAX,BAK in B cell homeostasis and prevention of autoimmune disease. *Proc. Natl. Acad. Sci. U.S.A.* **102**, 11272–11277 (2005).
19. C. T. Mayer *et al*., The microanatomic segregation of selection by apoptosis in the germinal center. *Science* **358**, eaao2602 (2017).
20. G. Knittel *et al*.; German International Cancer Genome Consortium Molecular Mechanisms in Malignant Lymphoma by Sequencing Project Consortium, B-cell-specific conditional expression of Myd88p.L252P leads to the development of diffuse large B-cell lymphoma in mice. *Blood* **127**, 2732–2741 (2016).
21. D. F. Robbiani *et al*., AID is required for the chromosomal breaks in c-myc that lead to c-myc/IgH translocations. *Cell* **135**, 1028–1038 (2008).
22. T. M. Yeh, S. J. Korsmeyer, J. M. Teale, Skewed B cell VH family repertoire in Bcl-2-Ig transgenic mice. *Int. Immunol.* **3**, 1329–1333 (1991).
23. A. D. Gitlin *et al*., Independent roles of switching and hypermutation in the development and persistence of B lymphocyte memory. *Immunity* **44**, 769–781 (2016).
24. M. M. Meredith *et al*., Expression of the zinc finger transcription factor zDC (Zbtb46, Btbd4) defines the classical dendritic cell lineage. *J. Exp. Med.* **209**, 1153–1165 (2012).
25. N. C. Shaner *et al*., A bright monomeric green fluorescent protein derived from Branchiostoma lanceolatum. *Nat. Methods* **10**, 407–409 (2013).
26. L. von Boehmer *et al*., Sequencing and cloning of antigen-specific antibodies from mouse memory B cells. *Nat. Protoc.* **11**, 1908–1923 (2016).
27. S. Moteki *et al*., Use of a designer triple expression hybrid clone for three different lipoyl domain for the detection of antimitochondrial autoantibodies. *Hepatology* **24**, 97–103 (1996).